Fault Localization and Failure Modes in Microsystems-Enabled Photovoltaic Devices

Benjamin B. Yang, Jose L. Cruz-Campa, Gaddi S. Haase, Paiboon Tangyunyong, Edward I. Cole Jr.,
Alejandro A. Pimentel, Paul J. Resnick, Murat Okandan, Gregory N. Nielson
Sandia National Laboratories
Albuquerque, NM
bbyang@sandia.gov

***Abstract* — Microsystems-enabled photovoltaic (MEPV) technology is a promising approach to lower the cost of solar energy to competitive levels. This paper describes current development efforts to leverage existing silicon integrated circuit (IC) failure analysis (FA) techniques to study MEPV devices. Various FA techniques such as light emission microscopy and laser-based fault localization were used to identify and characterize primary failure modes after fabrication and packaging. The FA results provide crucial information used in provide corrective actions and improve existing MEPV fabrication techniques.**

Keywords — microsystems-enabled photovoltaics; reliability; failure analysis

I. INTRODUCTION

Current photovoltaic (PV) technologies, namely wafer-silicon-based PV, thin film PV, and concentrated photovoltaics (CPV), are not yet cost competitive with traditional power sources due to various technological challenges. CPV has the highest efficiency and the highest cost. It requires accurate tracking mounts that significantly add to overall system costs. Thin-film PV is the least expensive technology, but suffers from low efficiency due to low carrier lifetimes. Wafer-silicon-based PV is the most popular PV technology due to its relatively high efficiency and reasonable cost. The manufacturing expense involved in wafer-based silicon, however, is dominated by material costs.

The microsystems-enabled photovoltaic (MEPV) approach utilizes microfabrication techniques to produce small and thin hexagonal silicon solar cells that are 250 μm to 2 mm in diameter and 14 μm to 20 μm in thickness. The fabricated units are released from the wafer and reassembled on a new substrate. This process allows the repurposing of silicon wafer material to manufacture additional cells, thus reducing the material costs that hinder wafer-silicon-based PV [1]. The reduced dimensions and fabrication approach also lead to higher energy densities—current efficiencies are up to 14.9% [2]. These efficiencies are the beneficiaries of scaling effects such as improved carrier collection and a decreased number of defects. The small size allows a wider range of applications such as implementation on flexible substrates [3]. Overall, the MEPV approach allows silicon-wafer-based PV to enjoy lower material costs and broader applications but without the penalty of thin-film PV's decreased efficiency or CPV's need for high-accuracy tracking mounts.

The development of FA techniques to improve the performance and reliability of MEPVs will further accelerate the advancement of this technology and improve the cost-competitiveness of solar energy. This paper describes current efforts to establish a failure analysis (FA) and reliability framework to complement existing work in the area. We explore failure modes affecting device yield through the use of light emission microscopy (LEM), light-induced voltage alteration (LIVA), and thermally-induced voltage alteration (TIVA).

II. MEPV TECHNOLOGY OVERVIEW

Each MEPV unit consists of p-doped and n-doped areas on crystalline silicon followed by deposition of insulating nitride layers and two metal 1 regions. One metal 1 region is connected to numerous circular-shaped p-doped areas through contacts that go through the nitride. Similar contacts connect the other metal 1 region to n-doped areas. Before the metallization, the MEPV is released through an HF etching step. The cells are then attached onto the final substrate silicon-side-up (metal-side-down).

Figure 1 shows the back side (metal-side-up, silicon-side-down) of an MEPV unit. The metalized portion of the left half of the MEPV, labeled with the letter "P", is connected to the p-doped regions of silicon. The right half, labeled with the letter "N", is connected to the n-doped regions. Both metal 1 pieces have fingers that are interlaced along the centerline of the MEPV. The four pillars in the figure are later connected to the final substrate with solder. The larger array of dots that are visible throughout the MEPV are the etch release holes. The smaller dots are the location of the contacts that connect the doped regions of the silicon to the metal 1 layer.

A cross section sketch of a p-doped region is shown in Figure 2. The n-doped region has a similar geometry. The various layers and geometries are not drawn to scale for the sake of clarity. Note that all metal layers lie beneath the silicon and doped regions. The thinness of the silicon substrate allows effective harvesting of the generated carriers with the metal 1 residing on the back side. Having all metal layers beneath the silicon eliminates shadowing and exposes the entire MEPV to the light source.

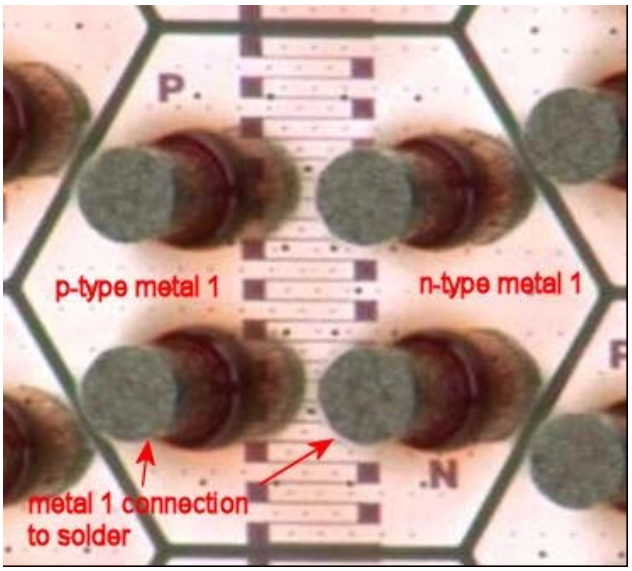

Figure 1: This metal-side-up, silicon-side-down picture of an MEPV unit shows the two pieces of metal 1 that are connected to either the p-doped (left half) and n-doped (right half) regions. The two metal 1 pieces have interlacing fingers that run along the center of the MEPV. The silicon beneath the metal 1 is visible between the fingers. The four pillars provide electrical connection to the substrate through a solder connection in a subsequent packaging step. Etch release holes, and the locations of contacts connecting the doped areas to the metal 1 layer are also visible.

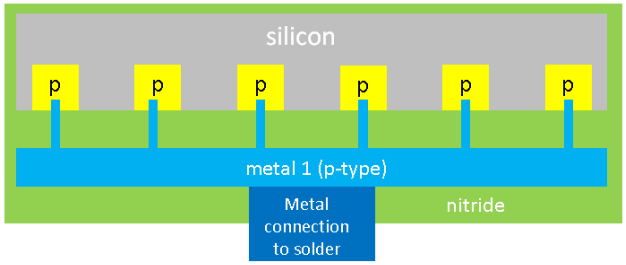

Figure 2: Cross section sketch of the p-type section of an MEPV unit. Critical connections include the contacts that connect the implantation regions to the metal 1 and the solder that connects the MEPV to the final substrate.

Since the p- and n-regions are isolated from the metal 1 through a nitride layer, reliable fabrication of the contacts that link them directly relate to performance. In addition, the solder that connects the metal to the final substrate is also a potential point of failure. The unique geometry of the MEPV also necessitates a new evaluation of the degradation mechanisms that may limit long-term performance.

III. Failure Analysis Techniques Overview

The project described in this paper aims to identify and characterize primary failure modes in MEPV devices and detect units prone to early failure. A variety of FA techniques are applied to cells that are nonfunctioning after fabrication. An initial emphasis is placed on atypically low-yielding arrays in order to study as many failure modes as possible.

The MEPV array is first characterized through measurement of its dark current-versus-voltage (I-V) curves and optical inspection. The functionality of each individual element is then evaluated through light emission microscopy (LEM). In LEM measurements, an MEPV is forward biased and the resulting light emission from the device is captured with a low-noise, cryogenically cooled camera. LEM not only separates functioning cells from nonfunctioning ones, but also allows qualitative evaluation of their relative performance. The intensity of light emitted by the device is directly proportional to the performance of the devices. Nonfunctioning devices will not emit light while functioning ones will have a strong emission.

We also explore the electrical response of a MEPV to lasers with wavelengths above and below the silicon band gap under various biasing conditions. In the case of the light-induced voltage alteration (LIVA) technique, the device is placed in either a forward or reverse biased configuration with a constant-current power supply. While biased, the device is locally illuminated with a raster-scanning laser beam that has a wavelength above the silicon band gap [4]. As the laser beam is scanned across the device, it interacts with the sample by creating electron-hole pairs and generating photo-current near electrical junctions. The induced voltage changes in the power supply in response to the photo-current production are recorded as a function of the scanning laser position to form an "induced voltage" or LIVA image.

Thermally-induced voltage alteration (TIVA) is similar to LIVA, except that the wavelength of the laser is below the band gap. As such, the laser no longer generates electron-hole pairs but will instead locally heat the laser-illuminated areas [4]. The resulting "induced voltage" or TIVA images can nondestructively identify low-resistance current leakage paths or areas of thermocouple-like activity in the device.

Following defect localization, subsequent destructive sample preparation techniques, such as focused ion beam (FIB) cross sectioning and mechanical polishing, coupled with scanning electron microscopy (SEM) imaging are used to determine the root cause of nonfunctioning or poorly-performing devices.

The reliability and FA efforts in this paper focus on identifying failure mechanisms and yield detractors in the fabrication and packaging process as well as exploring the use of techniques such as LEM, LIVA and TIVA to nondestructively identify them. These techniques can then be used as additional tools to monitor degradation as part of an ongoing study into the predicted reliability of MEPV technology.

IV. Results

The following subsections highlight the application of the LEM, LIVA and TIVA techniques for root cause analysis of yield detractors and evaluation of MEPV cell performance. Section IV.1 establishes the use of TIVA for localizing faulty connections between the silicon and metal 1. In Section IV.2, the application of LIVA and TIVA under different biasing conditions provides insight into the number of different failure modes that cannot otherwise be differentiated. LIVA was also used to suggest a correlation between uniformity of performance with overall module efficiency.

IV.1 Contact Evaluation with TIVA

As described in Figure 2, a high success rate in the fabrication of contacts connecting the metal 1 to the silicon implantation region is directly related to the performance of the MEPV. During earlier development of the MEPV, TIVA was successfully established as a technique to determine the connectivity of each individual contact.

Figure 3 illustrates the application of TIVA to evaluate contacts using a laser with a wavelength of 1340 nm. The left image in Figure 3 is a reflected bright field image of the region of interest. The metal 1 line in the center of the image is connected to n-doped regions of silicon in a radial design pattern. In the TIVA data of Figure 3, only the normal non-defective contacts are visible, enabling rapid evaluation and localization of defects. The TIVA signals in the non-defective contacts are the result of a thermocouple effect. This effect produces an electromotive force (EMF) and voltage change through an intact current path. Since defective contacts do not carry current, no TIVA signals are observed.

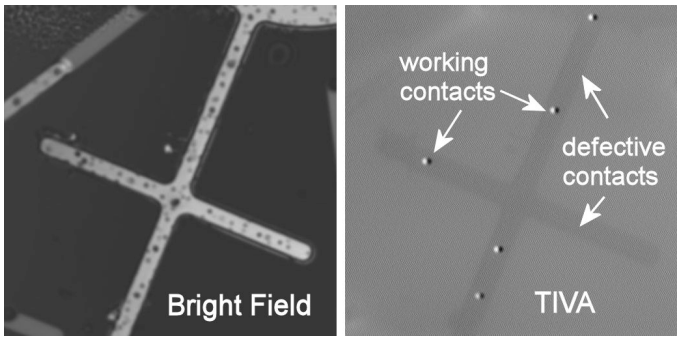

Figure 3: Example of using TIVA to identify defective connections between the implantation regions and the metal contacts below. The metal contacts are visible in the scanning laser bright field image. In the TIVA image, sites where the connection between the doped silicon and metal contact are faulty can easily be identified and isolated for further analysis.

Subsequent cross section at the failure sites identified that the root cause was over-etching during the release process that electrically isolated the contact from the implantation region. Figure 4 shows a SEM image of a FIB cross section that illustrates this failure mechanism. The etch-release process has since been optimized and is no longer a significant yield detractor.

IV.2 Packaging and Performance Evaluation with LIVA and TIVA

The connection between the MEPV and the substrate is accomplished through four solder sites shown in Figure 1. This packaging process and the associated challenges of evaluating the successful electrical connection of individual MEPV elements into the array is the subject of this subsection.

A combination of LEM, LIVA and TIVA are used to evaluate the operation of MEPV cells in an array. The response of the MEPV cells to these techniques under different biasing conditions provides insight into the number of types of failure mechanisms at play.

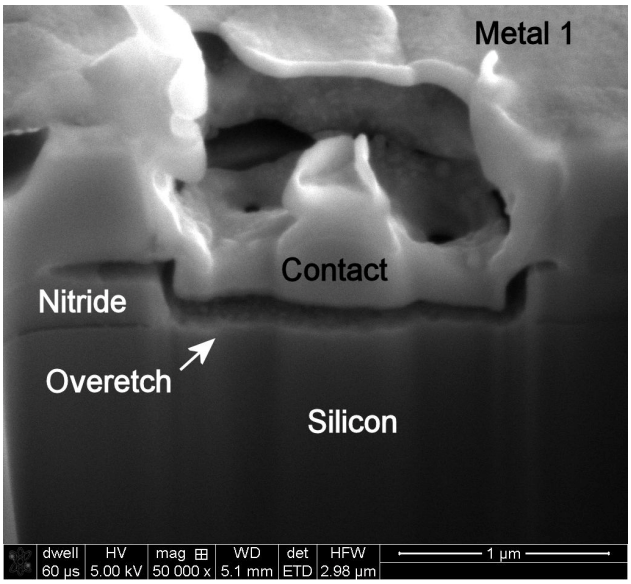

Figure 4: FIB cross section reveals an over etch that disconnects the metal from doped region

Both LEM and forward-biased LIVA have been used to identify nonfunctioning cells in MEPV arrays. Figure 5 shows an example of both functioning (cell A) and nonfunctioning cells (cell B and C) that were identified with LEM. LEM can be used not only to find nonfunctioning cells but also to identify those with diminished performance, which show up as darker regions on the cell.

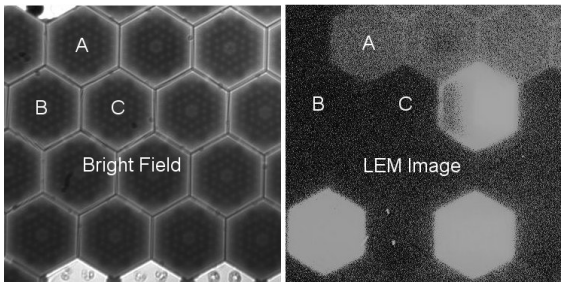

Figure 5: Example of an MEPV light emission microscopy image. The left figure shows the reflected bright field image of the examined area. The right shows the LEM image under forward bias where functioning cells emit photons that are captured by the camera. We can see that while cell A is functional, cells B and C are not.

Forward-biased LIVA provides similar information, as shown in Figure 6. For comparison purposes, the figure encompasses a similar area as Figure 5. We use near-band-gap (1064 nm) and above-band-gap (543 nm) wavelengths to perform LIVA. In reverse-biased LIVA, certain nonfunctioning cells appear in the image while others do not. This suggests different failing modes that can be categorized using the LIVA technique. In Figure 6, no LIVA signals were observed for cell C for both forward biased and reverse biased conditions. LIVA signals in cell B, however, appear in the reverse-biased LIVA image but not in the forward-biased image. This result also implies that cell B either has a weak photovoltaic response, or has a poor electrical connection to the substrate.

Figure 6: LIVA image of the same region as Figure 1. The left image is a scanning laser bright field image. The center picture is the forward biased LIVA image, showing that cell A is functioning while cells B and C are nonfunctioning. The right picture is the reversed biased LIVA image. Cell B has a weak response while cell C has none, suggesting different failure mechanisms.

Using a wavelength of 1340 nm, which has energy below the band-gap of the device, we find that the TIVA technique also has a different response in forward and reverse bias. Under forward bias, only functional cells appeared in the TIVA image. Similar to LIVA, we find that a subset of nonfunctioning cells appear in the TIVA image when under reverse bias. An example is cell B in Figure 7, which appears in the reverse-biased TIVA image, but not the forward-biased one. Unlike LIVA however, the TIVA image does not detect diffusion regions, but instead identifies resistive current paths that are sensitive to localized heating. The identical LIVA and TIVA response when under forward and reverse bias suggests that cell B may or may not have full photovoltaic functionality but indicates that it is hindered by a weak electrical connection to the substrate.

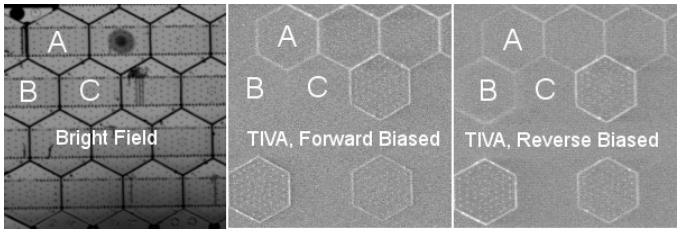

Figure 7: TIVA image of the same region the previous two figures. The left image is the scanning laser bright field image. Different features and defects are visible due to the longer wavelength. The forward-biased TIVA image shows that cell A is functioning while cells B and C are nonfunctioning. In the reversed-biased TIVA image, cell B has a weak response while cell C has none, suggesting that cell B has a different failure mechanism and is still electrically connected to the substrate.

LIVA has also been established to identify failure mechanisms in the electrical configuration of the MEPV. Figure 8 shows an example of an MEPV cell that is incorrectly connected. The 543 nm laser used to generate this figure scans from the right to the left. If the MEPV is connected incorrectly, the electrical response, and image contrast changes non-uniformly. In the Figure 8, the dark and bright edges of the incorrectly-connected MEPV cell on the lower-right mirror that of the functioning MEPV on the upper-left. This result suggests that the cell in question is biased differently than the rest of the array.

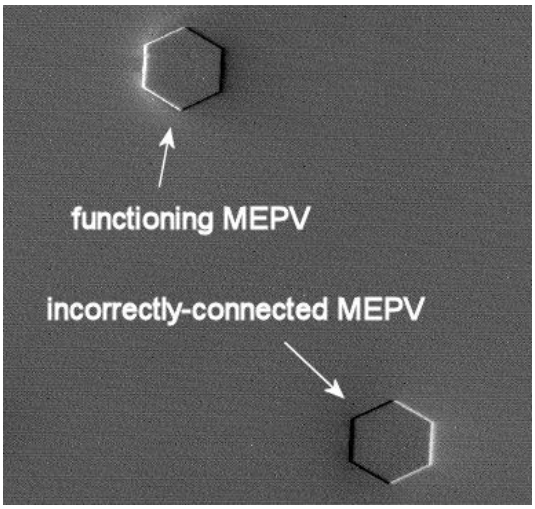

Figure 8: LIVA can be used to determine correct electrical connectivity of MEPV cells. The image above suggests that the MEPV on the lower-right is incorrectly connected, possibly causing it to be forward-biased when all other cells are reversed-biased.

LIVA was also used to establish a correlation between the uniformity in performance of MEPV cells fabricated from the same wafer and its overall efficiency. Figure 9 shows the LIVA response of an MEPV array under reverse bias. All cells in the array are fabricated from the same wafer. In this figure, the laser scans vertically from bottom to top. The MEPV cells in each horizontal row are connected in parallel and each of these rows are connected in series. The relative brightness of each row corresponds to the aggregate efficiency of each row relative to its neighbors, where brighter is indicative of increased performance. The LIVA image in Figure 9 shows that a majority of the performance takes place in the third, fourth, and eight rows from the top.

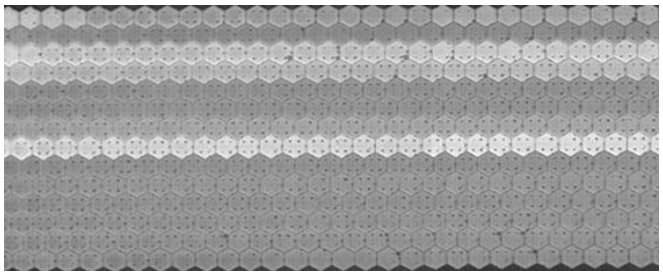

Figure 9: LIVA image of module with non-uniform performance from one horizontal row to the next. The third, fourth, and eighth rows from the top outperform the other rows.

A module with higher efficiency has a more uniform response across each of the rows. An example is the module shown in Figure 10, which is 1.86 times more efficient than the Figure 9 module. Therefore, the LIVA study suggests a correlation between cell-to-cell performance consistency in a wafer and the subsequent overall module efficiency.

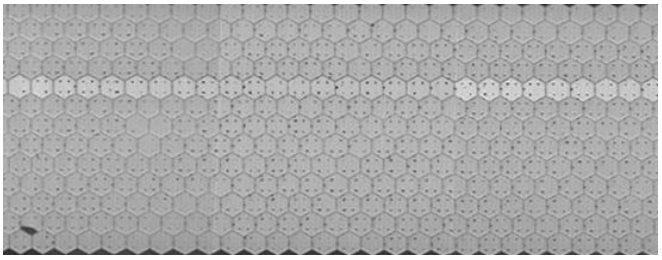

Figure 10: LIVA evaluation of a different module with more uniform performance compared to the previous figure. The module with more uniform row-to-row performance had 1.86 times higher efficiency, suggesting a correlation between cell-to-cell consistency and overall module efficiency.

V. SUMMARY

In this paper, we describe the capabilities of LEM, LIVA and TIVA under different biasing conditions to evaluate MEPV devices. TIVA was used to identify and help solve connectivity issues between the doped regions and metal contacts. LEM, LIVA and TIVA under different biasing conditions can locally evaluate the electrical and photovoltaic performance of an array of MEPVs. LIVA has also been shown to nondestructively identify MEPVs that were incorrectly connected. Subsequent study to correlate LIVA and TIVA response with failure mechanisms is ongoing. The findings will establish a system where LIVA and TIVA are used as a preliminary, nondestructive technique to identify potential failure mechanisms behind nonfunctioning or underperforming MEPV cells. This resulting collection of nondestructive techniques will be instrumental in reliability studies by serving as additional methods to monitor degradation.

The MEPV approach has been demonstrated to produce high-efficiency devices that have the potential to significantly enhance the cost competitiveness of solar energy. The findings and techniques in this paper form the foundation to a reliability program that functions in parallel with existing efforts to accelerate the progress of MEPV technology into a high-reliability, high-yielding product**.**

ACKNOWLEDGMENTS

Sandia National Laboratories is a multi-program laboratory managed and operated by Sandia Corporation, a wholly owned subsidiary of Lockheed Martin Corporation, for the U.S. Department of Energy's National Nuclear Security Administration under contract DE-AC04-94AL85000.

REFERENCES

[1] G. N. Nielson, M. Okandan, J. L. Cruz-Campa, A. L. Lentine, W. C. Sweatt, V. P. Gupta, and J. S. Nelson, "Leveraging scale effects to create next-generation photovoltaic systems through micro- and nanotechnologies," *Proceedings of SPIE*, vol. 8373, pp. 837317–837317, May 2012.

[2] J. L. Cruz-Campa, M. Okandan, P. J. Resnick, P. Clews, T. Pluym, R. K. Grubbs, V. P. Gupta, D. Zubia, and G. N. Nielson, "Microsystems enabled photovoltaics: 14.9% efficient 14 μm thick crystalline silicon solar cell," *Solar Energy Materials and Solar Cells*, vol. 95, no. 2, pp. 551–558, Feb. 2011.

[3] J. L. Cruz-Campa, G. N. Nielson, P. J. Resnick, C. A. Sanchez, P. J. Clews, M. Okandan, T. Friedmann, and V. P. Gupta, "Ultrathin Flexible Crystalline Silicon: Microsystems-Enabled Photovoltaics," *IEEE Journal of Photovoltaics*, vol. 1, no. 1, pp. 3 –8, Jul. 2011.

[4] E. I. Cole, M. R. Bruce, D. L. Barton, P. Tangyunyong, V. J. Bruce, C. F. Hawkins, J. M. Soden, C. L. Henderson, R. M. Ring, W.-L. Chong, D. H. Eppes, J. Wilcox, and D. A. Benson, "Optical tools and techniques for failure analysis of modern integrated circuits," in *The 16th Annual Meeting of the IEEE Lasers and Electro-Optics Society, 2003. LEOS 2003*, 2003, vol. 2, pp. 537– 538 vol.2.